Effect of Interface Shape on Advancing and Receding Fluid-Contact Angles around Spherical Particles

Nesrin Şenbil, Wei He, Vincent Démery, Anthony D. Dinsmore

Supplementary Information

In these supplementary materials, we explain our measurement methods in detail. Specifically we describe our methods of preparing glass spheres, imaging, extracting the contact angle by fitting to the interface shape, and we show a plot comparing the results of the fitting and 'geometric' methods. We then describe an experiment showing that the reduction of contact angle is not merely an image artifact arising from interface curvature. Finally, we describe our methods of measuring the contact-line shape.

Purchasing, Cleaning and Functionalizing the Glass Spheres:

Borosilicate glass spheres 1/8" (3.18 mm) in diam. were manufactured by Winsted Precision Ball Company and purchased from McMaster-Carr (cat. no. 8996K22). Spheres were washed in Nochromix® (Godax Laboratories), then rinsed with deionized water and dried in oven at 80 °C for 2 h. A thin rigid rod was then glued to the sphere with epoxy; this rod allowed us to manipulate the sphere. Finally we immersed the sphere in polydimethylsiloxane (PDMS; Gelest cat no. DMS-T22) at 150 °C for 24 h, following the method of Krumpfer *et al*. [S1]. Before starting each experiment, we washed the coated, rod-attached spheres with deionized water and dried them with flowing air.

AFM Measurements of a PDMS-coated Sphere:

Figure S1 shows an atomic force microscope (AFM) image and a resulting height profile of a PDMS-coated sphere. AFM measurements were done using an Asylum Research MFP-3D SA in non-contact mode with a Si tip (App Nano, Mountain View, CA; #ACT-R-W). The root-mean-square of the height is 13 nm. Micron-length scratches that are a few nm deep are seen, likely from the manufacturing process, but we found no evidence of directionality in the scratch pattern.

The Fitting Method of Finding the Contact Angle:

As described in the text, we used two methods to obtain the contact angle θ on the left and right sides of the target sphere, using the images. Here we provide further details on the fitting method.

The meniscus or deformation around a single ('target') sphere, placed in an initially flat interfaces, decays as $z(y)=A\ \ln(y\text{-}y_T)$ if $(y-y_T) << L_c$, where y_T is the center of the target sphere and L_c is the capillary length $(\gamma/g\rho)^{½}$. For a water-air interface, L_c = 2.7 mm. We use coordinates where the interface height is z, the sphere is centered at the origin, and the camera images the y-z plane (see Fig. 1(c) of the main text). If there is another, secondary, sphere at position y_S close to the target sphere, then the interface at the target sphere is no longer isotropic in shape and one expects an induced quadrupolar deformation [S2,S3] around the target sphere, proportional to $1/(y-y_T)^2$.

To fit the right-hand side of the target sphere (the side that is far from the secondary sphere), we fit the interface height to this function:

$$z(y) = A\ln(y-y_T) + B\ln(y-y_S) + C/(y-y_T)^2 + E, \quad \text{(S1)}$$

where A, B, C, and E are fit parameters. The first and second terms describe deformations surrounding each sphere and the third term describes the induced quadrupolar deformation around the target sphere because of the secondary sphere. We obtain good fits to this function within a distance of 2.7 mm.

To fit the left side of the target sphere (which is close to the secondary sphere), we must add an extra term to account for the fact that the target sphere induces a quadrupolar deformation about the secondary sphere. (This term becomes quite small on the far side of the target sphere so it was not included in the right-hand-side fit.) We fit the left section of the interface to the following function:

$$z(y) = A\ln(y-y_T) + B\ln(y-y_S) + C/(y-y_T)^2 + F/(y-y_S)^2 + E, \quad \text{(S2)}$$

and the values of the fit parameters (A, B, C, E, F) may be different from the right-hand side. The fourth term is added to account for the fact that target sphere can also induce quadrupole around the secondary sphere.

From the fitted shape of the interface, we extracted the tilt angle of the interface at the contact point. We then found the tilt angle of the sphere's surface at the contact point by superimposing a circle on the image of the sphere and finding the tangent at the contact. The contact angle θ was then calculated from these two angles.

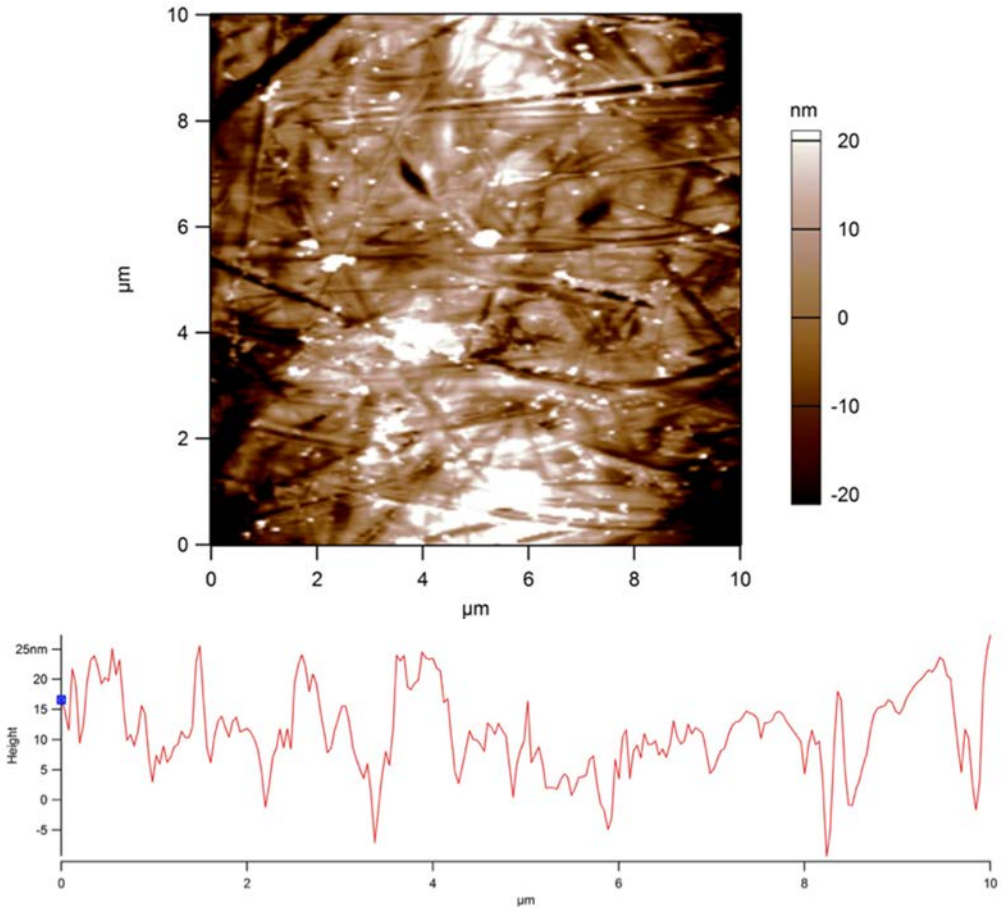

FIG S1: AFM image and height profile of PDMS-coated sphere.

This fitting method removes much of the opportunity for measurement bias and also gives a measurement that is independent of the geometric method (described in the main text). Fitting also allows us to verify that the interface shape is as expected and indicates the lack of contaminants or defects that perturb the interface shape (which we also checked for directly).

In Fig. S3, we compare contact angles found from both methods. The results are in agreement and in both cases the drop of receding angle is approximately 11° as D_0 increases from zero to 0.13 mm^{-1}.

Saddle and Cylindrical Interfaces:

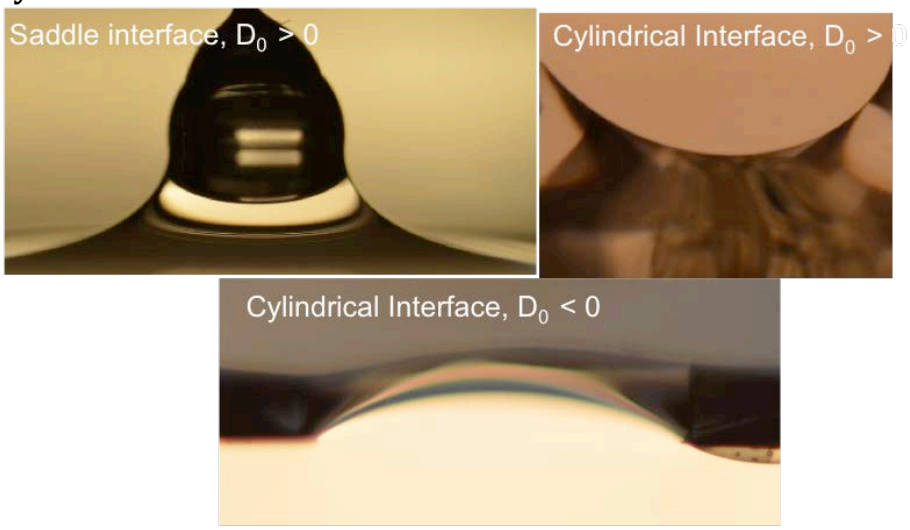

FIG S2: Saddle and cylindrical interfaces, before placing the target sphere.

Measuring Deviatoric Curvature:

At a given position on the interface in the image plane, one principal curvature lies in the image plane and was calculated from our fit to the interface height, $z(y)$: $c_1 = (d^2z/d^2y)/(1+(dz/dy)^2)^{3/2}$. The value of c_2 could not be measured directly from the image. Instead, we found c_2 from the constraint that the mean curvature, $H \equiv (c_1+c_2)/2$, determines the Laplace pressure, which must balance the gravitational pressure: $2\gamma H = \rho g(z-z_f)$, where γ is the air-water interfacial tension (72 mN/m), ρ is the mass density of water, g is the acceleration due to gravity, and z_f is the interface height far from the spheres where the interface was flat. Typical uncertainty of D_0, predominantly from z_f, was approximately 0.006 mm^{-1}.

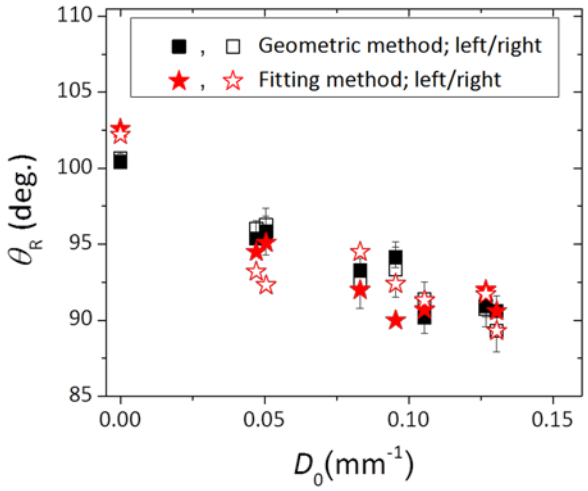

FIG. S3: Comparison of the geometric method with the fitting method.

A Geometric Control Measurement:

When the target sphere was very close to or in contact with a hydrophilic sphere, an

upward displacement of the target sphere caused the contact to recede on the far (right) side but to *advance* on the near (left) side. (Presumably, the contact was forced upward on the left side because of the contact-angle condition on the hydrophilic sphere.) In one such experiment, for example, we measured $\theta = 75°$ on the right-hand (receding) side and 108° on the left (advancing) side. These values are consistent with the fact that the contact visibly receded and advancing, respectively, at those positions. In this experiment, the reduction of θ_R on the right-hand side was even more pronounced than in the other experiments, which we attribute to the fact that the deviatoric curvature D_0 was greater because of the closer proximity to the secondary sphere. On the left-hand side, the curvature is substantial, yet we found an (advancing) angle indistinguishable from the flat-interface case, consistent with all of our data. This experiment serves as a control measurement, showing that the reduction of θ does not arise merely from an optical or imaging artifact associated with strong interface curvature: the result depends on whether the interface was advancing or receding.

Obtaining Contact-Line Coordinates:

In order to obtain pixel values of points such as interface or contact line around the sphere we used the Find Edges algorithm in ImageJ [S4], followed by an intensity threshold. All processing steps were verified by eye.

We observed the near side of the contact line (corresponding to $-\pi/2 < \phi < \pi/2$). The (y,z) coordinates of these points were extracted from the image and then converted into 3D coordinates using the known size and position of the sphere. We then fit the height of the contact line to a multipole expansion in polar coordinates (ρ,ϕ):

$$z(\varphi) = z_0 + z_1 \sin(\varphi) + z_2 \cos(2\varphi) + z_3 \sin(3\varphi) + z_4 \cos(4\varphi) + z_5 \sin(5\varphi), \qquad \text{(S3)}$$

where z is the measured height of the contact line, z_n are best-fit constants, and ϕ is the polar angle ($\phi = 0$ defines the x-axis, which points out of the page, and $\phi = \pi/2$ defines the right-hand side of the sphere). This function satisfies the reflection symmetry $z(\phi)=z(\pi-\phi)$, which accounts for the fact that our experimental system has reflection symmetry about the image plane.

Figure S2 shows that the contact line at the initially planar interface has a nearly constant height (*i.e.*, a circular ring shape), whereas the presence of the second sphere introduces tilt (z_1) and undulation (z_2, z_3, etc.).

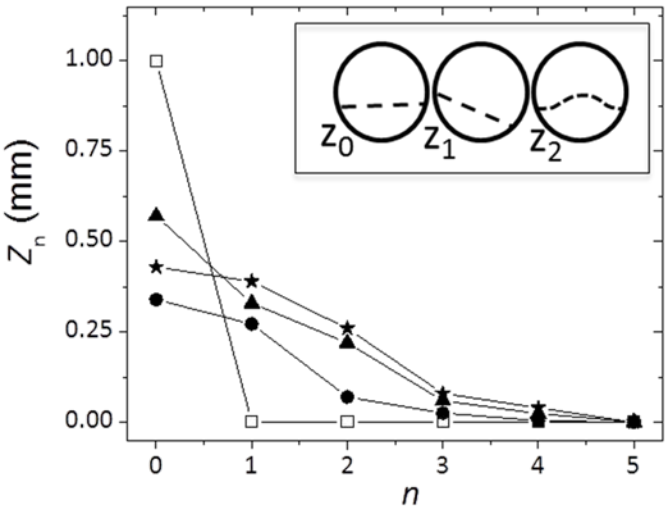

FIG. S4: Coefficients, z_n of the multipole expansion of the contact-line shape for initially planar interface (□; $D_0 = 0$), and anisotropic interfaces (●: $D_0 = 0.05$. ▲: $D_0 = 0.08$. ★: $D_0 = 0.13$ mm^{-1}).

References:

[S1] J. W. Krumpfer and T. J. McCarthy, "Contact angle hysteresis: a different view and a trivial recipe for low hysteresis hydrophobic surfaces," *Faraday Discuss.* **146**, 103 (2010).

[S2] A. Wurger, "Curvature-induced capillary interaction of spherical particles at a liquid interface," *Phys. Rev. E* **74**, 041402 (2006).

[S3] C. Zeng, F. Brau, B. Davidovitch, and A. D. Dinsmore, "Capillary Interactions among Spherical Particles at Curved Liquid Interfaces," *Soft Matter* **8**, 8582 (2012).

[S4] W. S. Rasband, (U. S. National Institutes of Health, Bethesda, Maryland, USA, 1997-2011).